03,10

Investigation of nanostructured thermoelectric materials on basis of SiGe

© Yu.I. Shtern[1], M.S. Rogachev[1,¶], M.Yu. Shtern[1], A.A. Sherchenkov[1], N.Yu. Tabachkova[2], V.P. Panchenko[1], M.V. Voronov[1], B.R. Mustafoev[1]

[1] National Research University of Electronic Technology, Moscow, Russia
[2] National University of Science and Technology, „MISiS", Moscow, Russia

E-mail: m.s.rogachev88@gmail.com

Received April 30, 2025
Revised September 17, 2025
Accepted January 12, 2026

Thermoelectric materials on basis of n- and p-type SiGe have been synthesized using mechanochemical synthesis and induction melting. Bulk samples were prepared from the powders of the synthesized materials by hot pressing and nanostructured samples by spark plasma sintering. Mechanical, thermal and electrophysical properties of the materials were studied, and thermoelectric figure of merit was determined. Properties of materials obtained by hot pressing and spark plasma sintering were compared. It has been established that the thermal conductivity of nanostructured materials decreases by up to 25 % due to phonon heat transport. This allowed increasing the maximum value of the thermoelectric figure of merit in the temperature range of 1070−1170 K for nanostructured materials based on SiGe of both types of conductivity — for *n*-type up to 1.24 ± 0.13 and *p*-type up to 1.22 ± 0.12.

Keywords: thermoelectricity, SiGe, nanostructuring, physical parameters, thermoelectric figure of merit.

DOI: 10.61011/PSS.2026.01.63231.103-25

1. Introduction

Recently, there has been a significant increase in interest in thermoelectric devices [1–4]. This is due, among other things, to the fact that one of the important modern scientific directions is the creation of alternative energy sources and energy-efficient technologies. In this regard, thermoelectric generators (TEG) are of great interest and are actively being developed [1,5,6]. Deep space exploration is an extremely important area of application of TEG. In this case, radioisotope TEG (RITEG) are used, in which the heat generated by the decay of radioactive materials is converted into electrical energy. A promising area of use of autonomous electric energy sources based on RITEG is their application in the development of remote areas of the Far North and the Far East, including the Northern Sea Route, isolated from centralized power supply systems.

However, the relatively low efficiency of the TEG leads to the fact that such devices are used mainly where autonomy, reliability and high operating life of the device are more important. The efficiency of thermoelectric generators is determined by the efficiency η:

$$\eta = \frac{T_{\text{hot}} - T_{\text{cold}}}{T_{\text{hot}}} \cdot \frac{\sqrt{(1 + Z\bar{T})} - 1}{\sqrt{(1 + Z\bar{T})} + T_{\text{cold}}/T_{\text{hot}}} \qquad (1)$$

where T_{hot} is the temperature of the hot junction of the thermoelement (TE); T_{cold} is temperature of the TE cold junction; $\bar{T} = (T_{\text{hot}} + T_{\text{cold}})/2$; Z is thermoelectric figure of merit of the semiconductor materials used.

Thermoelectric figure of merit determines the efficiency of semiconductor thermoelectric materials used to manufacture legs of *n*- and *p*-types of thermoelements:

$$Z = s^2\sigma/\kappa, \qquad (2)$$

where s is Seebeck coefficient, σ is electrical conductivity, κ is thermal conductivity of the material.

Thus, to increase the efficiency of the TEG, it is necessary to increase the Z of the thermoelectric materials used and the temperature difference (ΔT) between the TE hot and cold junctions and, accordingly, increase the TE operating temperature range.

Currently, thermoelectric materials have been developed that cover the entire temperature range from 200 to 1200 K, which is of interest for thermoelectric energy conversion. However, for all thermoelectric materials Z has a significant temperature dependence with a fairly sharp maximum at certain temperatures.

The thermoelectric materials currently used for practical purposes have a maximum value of $ZT \sim 1$. At the same time, in order to significantly increase the efficiency of TEG, it is necessary to significantly increase the thermoelectric figure of merit of materials.

The best high-temperature thermoelectric materials currently in use in the range of 900−1200 K are solid solutions based on SiGe of *n*- and *p*-types of conductivity, usually produced by classical methods, for example, hot pressing [7–9]. The thermoelectric figure of merit of high-temperature materials is lower than that of medium-

temperature materials. However, the ability to obtain significant temperature differences between hot and cold junctions of thermoelements, as well as the presence of sufficiently compact heat sources in the form of nuclear reactors, make the high-temperature range quite attractive. At the same time, advances in nanotechnology open up new opportunities in the search for promising thermoelectric materials and structures based on them. One of the currently actively developing areas for improving the thermoelectric figure of merit of materials is the development of nanostructured materials, including those based on SiGe [7–12]. However, the technology of nanostructured thermoelectric materials is still far from being widely used in practice.

In connection with the above, the purpose of this paper was to obtain, study and compare the properties of $Si_{0.8}Ge_{0.2}$ (1.8 wt.% P) *n*-type and $Si_{0.8}Ge_{0.2}$ (0.8 wt.% B) of *p*-type produced by the classical method and nanostructuring.

2. Experimental part

Synthesis of solid solutions of $Si_{0.8}Ge_{0.2}$ (1.8 wt.% P) *n*-type and $Si_{0.8}Ge_{0.2}$ (0.8 wt.% B) *p*-type was carried out by induction melting (IM) in an Indutherm VTC 200 V vacuum casting machine. The starting materials Si (99.999 wt.%) and Ge (99.999 wt.%), as well as dopants in a stoichiometric composition, were loaded into a ceramic crucible with a graphite inner coating. The crucible was then heated to a temperature of 1700 K in an Ar atmosphere. The molten material was kept at this temperature for 10 min.

In addition, thermoelectric materials based on SiGe, along with the induction melting method, were obtained using mechanical alloying (MA). This method is based on the principle of mechanical activation of a chemical reaction between the initial components. The initial Si and Ge components were ground to a size of no more than 2 mm. After that, additional grinding of these materials was carried out in a planetary ball mill (PBM) „Activator 2S“ to particle sizes not exceeding 100 nm. The initial components were loaded and unloaded in an inert atmosphere. For mechanical alloying, the obtained Si and Ge powders were poured into the grinding jars of a planetary ball mill „Retsch 400 PM“ in the required stoichiometric ratio, with the addition of dopants. The mechanical alloying was carried out cyclically to avoid overheating of the jars. Each cycle included rotating the jars for 30 min at a planetary disk speed of 400 rpm and stopping for 10 min. A total of 44 cycles were used, the total process time was 29 h.

The production of thermoelectric materials by hot pressing (HP) was carried out as follows. Ingots of solid solutions were ground to a particle size of $0.25-0.50$ mm. The resulting powder was hot pressed using an IP-2500M hydraulic press at a temperature of 1370 K and a pressure of 120 MPa for 5 min.

The technology for obtaining nanostructured thermoelectric materials was as follows. The materials synthesized by induction melting were ground to a particle size not exceeding 500 μm. Next, the resulting powder was additionally ground in a Retsch PM400 MA high-energy planetary ball mill. The rotation speed of the planetary disk was 400 rpm, the grinding time was 50 min. Next, the obtained nanodisperse powders were compacted by spark plasma sintering (SPS) using SPS 511S system with an electric current of the order of 1200 A in a pulsed mode with a pulse duration of up to 12 ms and intervals of 2 ms. The sintering time was 10 min, temperature was 1 373 K and pressure was 50 MPa.

In addition, bulk nanostructured materials were obtained from nanodisperse SiGe powders obtained as a result of mechanical alloying. Spark plasma sintering of powders was carried out under the conditions indicated above. The designation of the samples $Si_{0.8}Ge_{0.2}$, taking into account the methods of their preparation, is presented in Table 1.

The phase analysis of the studied materials was performed by X-ray diffraction using a Bruker B8 diffractometer equipped with a position-sensitive LYNXEYE detector. Monochromatized Cu Kα-radiation ($\lambda = 0.154$ nm) was used. The sizes of crystallites [13] were determined by the broadening of diffraction maxima. The compositions of the solid solutions were determined by the parameters of the crystal lattice. A detailed study of the structure of powders and bulk materials was carried out using an JEM-2100 transmission electron microscope at an accelerating voltage of 200 kV.

The density of the materials was measured by hydrostatic weighing based on Archimedes' law. The average density value was determined from 3 measurements with an error of no more than 0.01 g/cm^3.

To determine the mechanical properties of the materials, their Vickers microhardness was measured using a PMT-3M microhardness tester based on the recovered indenter print. A diamond pyramid with an angle at the top 136° was used as an indenter. The Vickers hardness value was calculated using the formula:

$$HV = 1.8544 \cdot \frac{P}{d^2}, \tag{3}$$

where P is the normal load applied to the indenter; d is the diagonal of the indenter imprint in the material. The average value of the print diagonals was calculated based on the results of at least 4 indentation experiments. The statistical error of measuring microhardness did not exceed 4 %.

The results of measuring the Hall constant on HMS-5000 (Ecopia) system at 300 K in a magnetic field of 0.55 T, at a current of 10 mA were used to determine the concentration and mobility of charge carriers. Samples with dimensions $7 \times 7 \times 2$ mm^3 were prepared for the studies. The concentration of the main charge carriers (n) and their mobility (μ)

Table 1. Samples $Si_{0.8}Ge_{0.2}$

Composition	Method of synthesis	Method of compaction	Designation
$Si_{0.8}Ge_{0.2}$ (1.8 wt.% P)	IM	–	SiGeP-IM
$Si_{0.8}Ge_{0.2}$ (0.8 wt.% B)		–	SiGeB-IM
$Si_{0.8}Ge_{0.2}$ (1.8 wt.% P)	MA	–	SiGeP-MA
$Si_{0.8}Ge_{0.2}$ (0.8 wt.% B)		–	SiGeB-MA
$Si_{0.8}Ge_{0.2}$ (1.8 wt.% P)	IM	HP	SiGeP-IM-HP
$Si_{0.8}Ge_{0.2}$ (0.8 wt.% B)			SiGeB-IM-HP
$Si_{1.8}Ge_{0.2}$ (1.8 wt.% P)		SPS	SiGeP-IM-SPS
$Si_{0.8}Ge_{0.2}$ (0.8 wt.% B)			SiGeB-IM-SPS
$Si_{0.8}Ge_{0.2}$ (1.8 wt.% P)	MA	SPS	SiGeP-MA-SPS
$Si_{0.8}Ge_{0.2}$ (0.8 wt.% B)			SiGeB-MA-SPS

were determined as follows:

$$n = 1/eR_{\mathrm{H}}; \quad \mu = \sigma R_{\mathrm{H}}, \tag{4}$$

where R_{H} is the Hall constant, e is the electron charge. The error in determining the Hall constant is 5%.

A previously developed technique and a measuring complex for its implementation was used to measure the thermoelectric parameters of materials in the temperature range from 300 to 1200 K [14]. The studies were carried out in a stationary mode in a single measuring cycle, the thermal conductivity was determined by the absolute method.

Electrical conductivity, Seebeck coefficient, and thermal conductivity were calculated using the formulas:

$$\sigma = \frac{2LI}{S(U_1 + U_2)}, \tag{5}$$

where I is the DC current passing through the sample; U_1 and U_2 — voltage drop across the sample at opposite current directions; L is the sample height; S is the sample cross-sectional area.

$$s = E/\Delta T, \tag{6}$$

where E is the measured thermoEMF value on the sample;

$$\kappa = LQ/(S\Delta T), \tag{7}$$

where Q is the heat flow through the sample; ΔT is the temperature difference on the sample.

The error of the method is 3% for the coefficients of Seebeck and electrical conductivity, 5% for the coefficient of thermal conductivity. The error calculation is described in Ref. [14].

3. Results and discussion

The method of grinding SiGeP-IM and SiGeB-IM in a planetary ball mill has been optimized for manufacturing bulk nanostructured thermoelectric materials, which makes it possible to obtain powders with a particle predominance of less than 100 nm. The dependence of the average size of the crystallites of powders on the grinding time at the rotation speed of the planetary disk 400 rpm is shown in Figure 1.

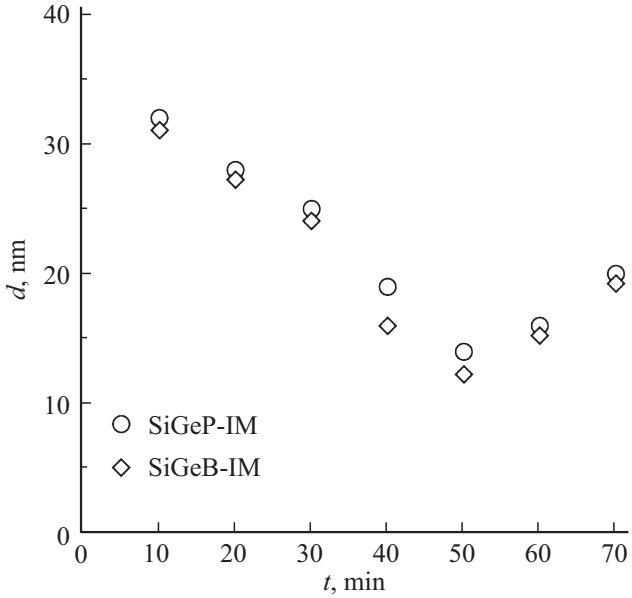

Figure 1. Dependences of the average particle size of SiGeP-IM and SiGeB-IM powders on the grinding time.

It has been established that the minimum powder sizes are achieved at a grinding time of 50 min and a rotation speed of 400 rpm of the planetary disk. A further increase in the grinding time leads to an increase in the average size of the crystallites of powders, which is associated with the agglomeration of the powder. An increase in the rotation speed of the planetary disk leads to a noticeable increase in

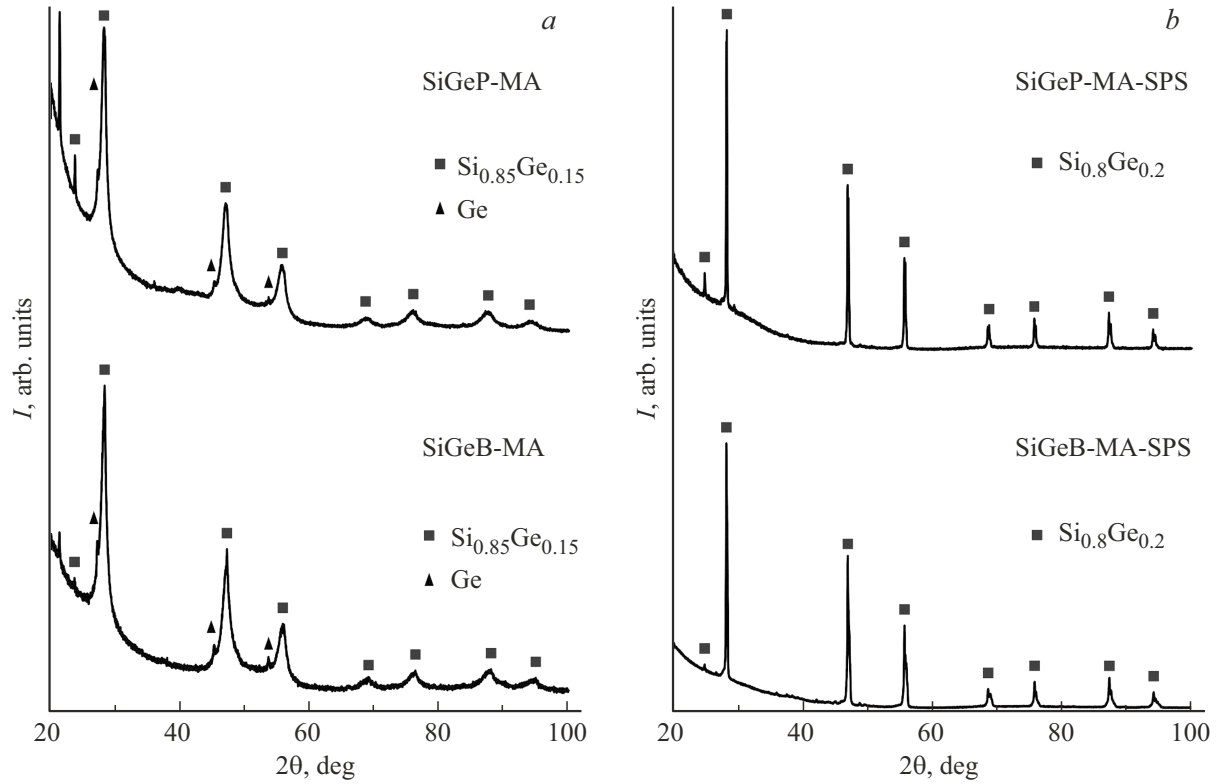

Figure 2. Diffraction patterns (*a*) of powders of SiGeP-MA and SiGeB-MA and (*b*) nanostructured SiGeP-MA-SPS and SiGeB-MA-SPS.

Table 2. Density and microhardness of thermoelectric materials

Material	ρ, g/cm^3	HV
SiGeP-IM	2.99	1101.3
SiGeB-IM	2.99	1097.1
SiGeP-IM-HP	2.92	1100.1
SiGeB-IM-HP	2.92	1087.1
SiGeP-IM-SPS	2.94	1109.0
SiGeB-IM-SPS	2.94	1099.9
SiGeP-MA-SPS	2.94	1108.2
SiGeB-MA-SPS	2.94	1099.4

the temperature of the powder during the grinding process, which also intensifies the agglomeration processes. The sizes of SiGe particles and agglomerates of *n*- and *p*-types do not differ significantly: for SiGeP-IM the average size of crystallites was 14 ± 2 nm, for SiGeB-IM — 12 ± 2 nm.

Table 2 presents the results of measuring the density and microhardness of synthesized and nanostructured thermoelectric materials.

The developed technology for compacting the obtained powders of materials using the SPS method ensures the density of nanostructured materials, which is 98 % of the density of materials obtained by direct fusion of components (theoretical density). The results of the microhardness measurement showed that this parameter is even slightly higher for nanostructured materials compared to classical materials. This result is consistent with the literature data for other nanostructured thermoelectric materials [15] and is important for the manufacture and operation of thermoelements.

As a result of the study of the phase composition of synthesized thermoelectric materials obtained by induction melting and mechanical alloying, it was found that in addition to the solid solution of SiGe, the Ge phase was present. At the same time, the phase composition of materials after SPS and HP changed; during sintering, the Ge phase dissolved in a solid solution, which was observed in powders after grinding. That is, after compaction, the presence of the Ge phase was not observed. Diffraction patterns of SiGeP-MA and SiGeB-MA powders, and nanostructured bulk SiGeP-MA-SPS and SiGeB-MA-SPS are shown as an example in Figure 2.

Table 3 shows the parameters of nanostructured thermoelectric materials.

The phase composition of the solid solution, determined from the data on the lattice parameters, corresponds to $Si_{0.8}Ge_{0.2}$. Based on the results of TEM, it was found that the structure of the samples is finely dispersed. Figures 3 and 4, as an example, show images of the sample structure SiGeP-MA-SPS and SiGeB-MA-SPS.

Table 3. Parameters of nanostructured SiGe samples

Sample	Average size of crystallites, nm	Microdeformations, %	Periods lattices, Å	Composition
SiGeP-IM-SPS	79 ± 5	0.021 ± 0.05	5.475 ± 0.001	$Si_{0.8}Ge_{0.2}$
SiGeB-IM-SPS	78 ± 5	0.058 ± 0.05	5.474 ± 0.001	$Si_{0.8}Ge_{0.2}$
SiGeP-MA-SPS	82 ± 5	0.025 ± 0.05	5.475 ± 0.001	$Si_{0.8}Ge_{0.2}$
SiGeB-MA-SPS	80 ± 5	0.060 ± 0.05	5.474 ± 0.001	$Si_{0.8}Ge_{0.2}$

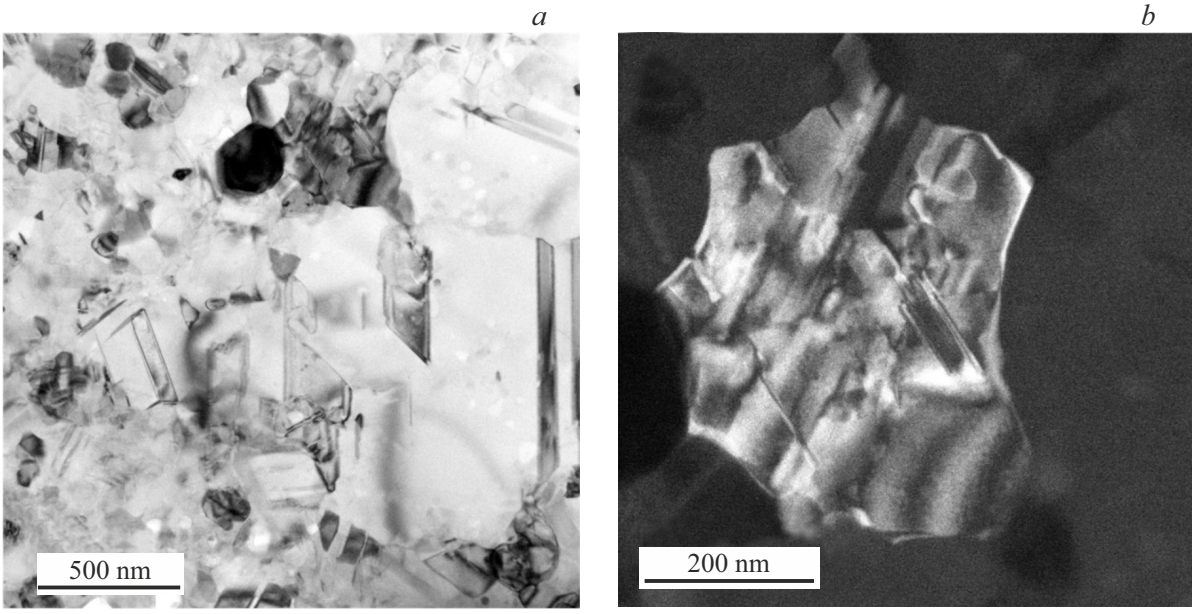

Figure 3. (*a*) TEM image of the SiGeP-MA-SPS structure, (*b*) TEM image of the SiGeP-MA-SPS crystallite.

The grain size in the SiGeP-MA-SPS sample varies mainly from 50 to 500 nm. The average grain size is ~ 80 nm, which coincides with the average crystallite size in these samples. The grains are quite perfect, there are no dislocations inside the grains. However, twins are quite common (regions in a crystallite with a naturally altered orientation of the crystal structure). An image of a single grain containing twin boundaries is shown in Figure 3, *b*. The location of the reflexes on the electron diffraction pattern corresponds to the solid solution of SiGe. Also, based on the results of TEM, it was found that the structure of the SiGeP-IM-SPS sample had a similar character.

The structure of this sample is more uniform compared to SiGeP-MA-SPS. The crystallite sizes are of the order of 80 nm. In addition to the twins, no other visible defects were observed in the structure of SiGe solid solutions. Individual grains of size $10-20$ nm were found in these samples. According to the TEM data, there are no pores along the grain boundaries or inside the grain. Analogous structural studies conducted for the SiGeB-IM-SPS sample showed similar results.

For thermoelectric materials obtained by HP and SPS, which are used for the manufacture of thermoelements, studies of thermal and electrophysical properties and their comparative analysis have been carried out. The results of the study are shown in Figures 5–9. Figures 5 and 6 show the results of a study of the temperature dependences of electrical conductivity and Seebeck coefficient of thermoelectric materials.

The general nature of the temperature dependences of both electrical conductivity and Seebeck coefficient indicates that all thermoelectric materials are partially degenerate semiconductor materials in the operating temperature range. The decrease in electrical conductivity with increasing temperature can be explained by the intermetallic nature of thermoelectric materials [16]. As the temperature increases in the operating temperature range, the concentration of the main carriers practically does not change, and the electrical conductivity decreases due to the scattering of charge carriers by lattice vibrations. An increase in the contribution of minority carriers, and a corresponding increase in the total carrier concentration at the end of the operating

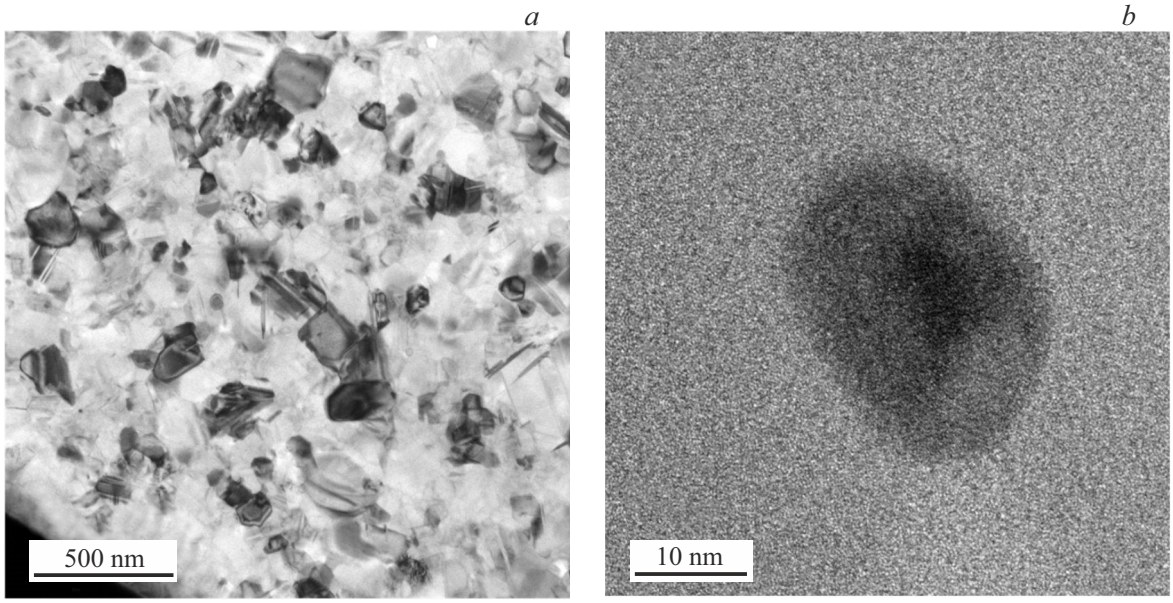

Figure 4. (*a*) TEM image of the SiGeB-MA-SPS structure, (*b*) TEM image of the SiGeB-MA-SPS crystallite.

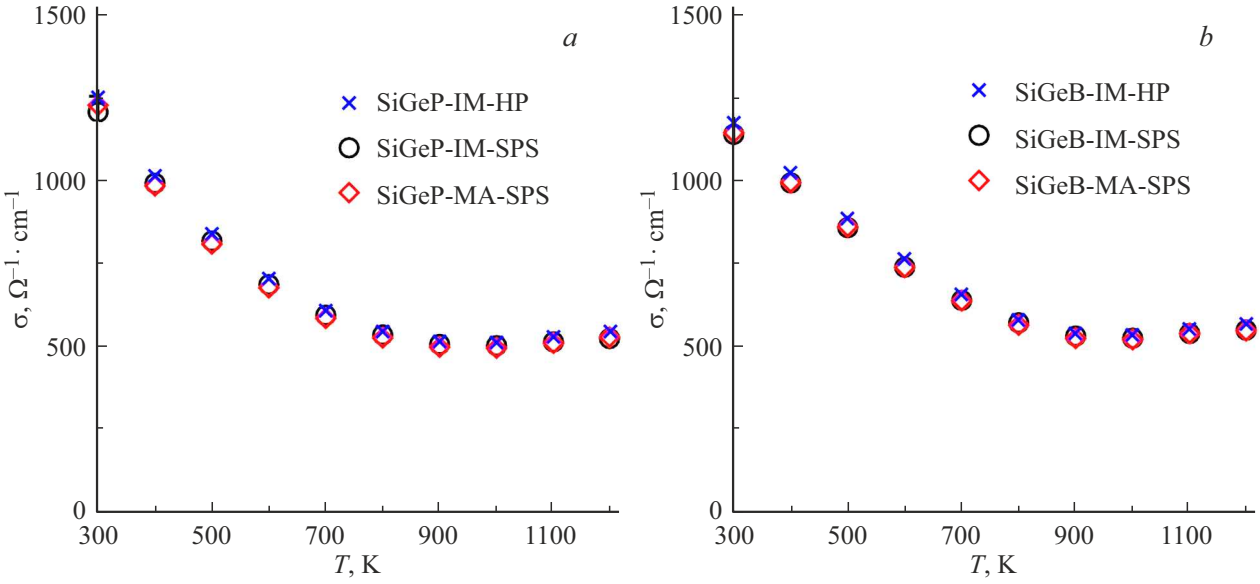

Figure 5. Temperature dependences of the electrical conductivity of thermoelectric materials of (*a*) *n*-type and (*b*) *p*-type.

temperature range, leads to a stabilization of electrical conductivity values and even a tendency to its growth. This characterizes the beginning of intrinsic conductivity. An increase in electrical conductivity correlates with a decrease in Seebeck coefficient at these temperatures, which confirms the influence of minority charge carriers on the mechanism of electrical transport.

The electrical conductivity of nanostructured thermoelectric materials over the entire temperature range is lower than for samples obtained by hot pressing by an amount not exceeding 2–4%. This is explained by the fact that nanostructured materials have slightly lower charge carrier mobility due to scattering on nanoscale inhomogeneities (Table 4).

As the temperature increases, the Seebeck coefficent for the studied thermoelectric materials increases, reaching a maximum of 250 μV/K and even slightly more at temperatures of 1000–1100 K (Figure 6). The observed decrease in Seebeck coefficient at the end of the operating temperature range is also associated with an increase in the contribution of minority charge carriers to the electrical transport process. It should be noted that Seebeck coefficient is more sensitive to the influence of minority carriers, since its decrease begins at 10–15 K before the increase in electrical

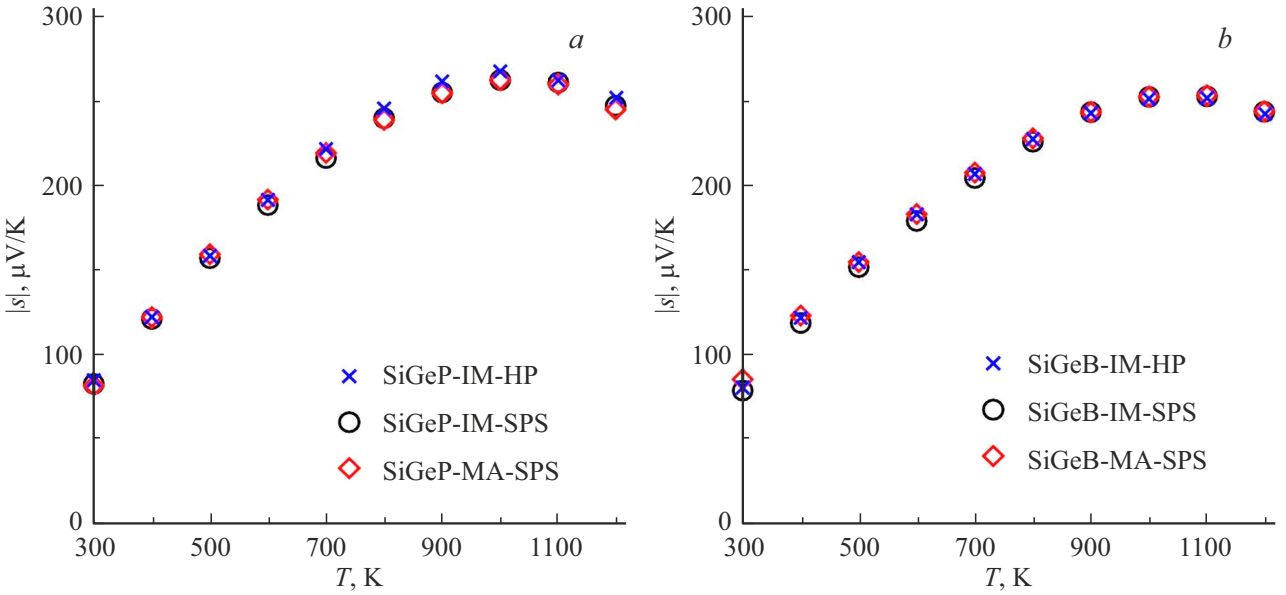

Figure 6. Temperature dependences of Seebeck coefficient of thermoelectric materials of (*a*) *n*-type and (*b*) *p*-type.

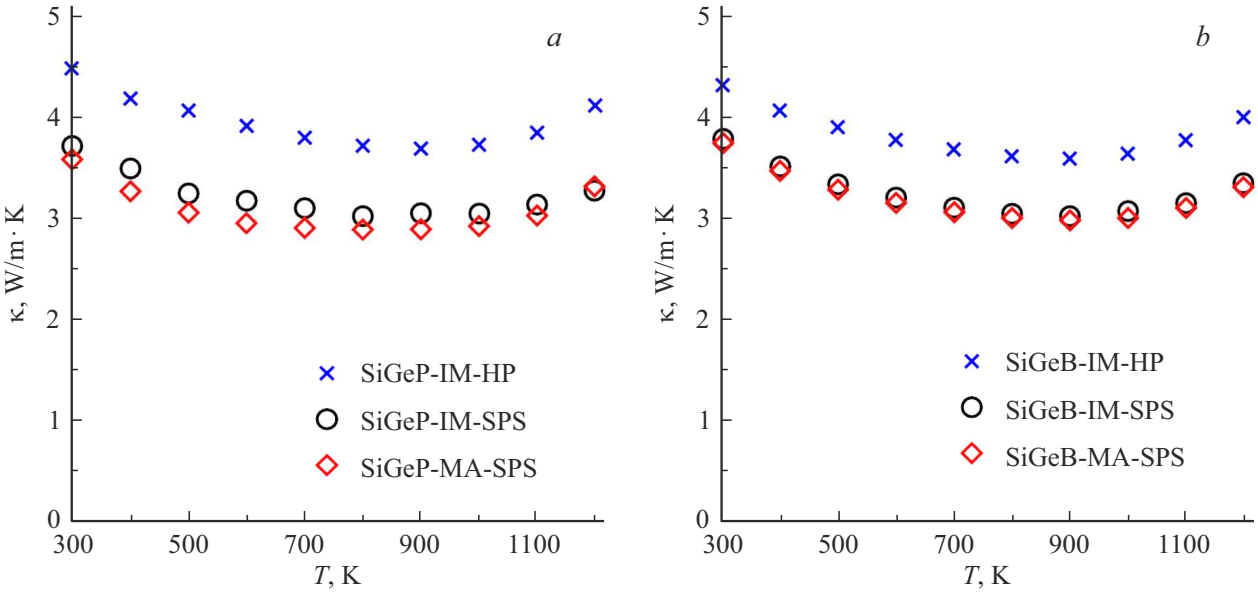

Figure 7. Temperature dependences of thermal conductivity of thermoelectric materials of (*a*) *n*-type and (*b*) *p*-type.

Table 4. Concentration and mobility of charge carriers of thermoelectric materials

Material	n, 10^{19} cm^{-3}	μ, cm^2/V · s
SiGeP-MA-SPS	27.24	27.4
SiGeB-MA-SPS	28.72	24.3
SiGeP-IM-SPS	27.28	26.9
SiGeB-IM-SPS	28.75	24.6
SiGeP-IM-HP	26.94	27.9
SiGeB-IM-HP	28.46	24.8

conductivity. The difference in the Seebeck coefficient values of nanostructured and hot-pressed materials does not exceed the measurement error.

The results of the Hall coefficient study, as well as data on electrical conductivity, made it possible to determine the concentration of charge carriers (n) and their mobility (μ) (Table 4).

The carrier mobility of nanostructured thermoelectric materials is lower than that of materials obtained by pressing by no more than 3 %, which is explained by their additional scattering on the nanodisperse elements of the structure [17].

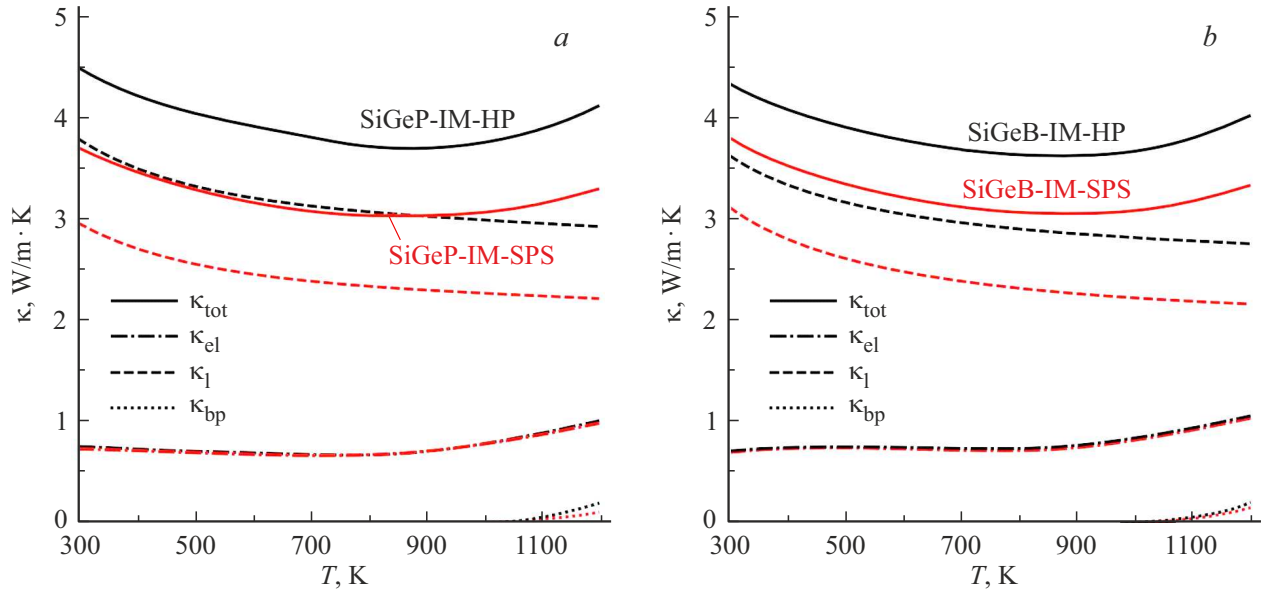

Figure 8. Temperature dependences of κ_{tot} and its components for thermoelectric materials of (*a*) *n*-type and (*b*) *p*-type.

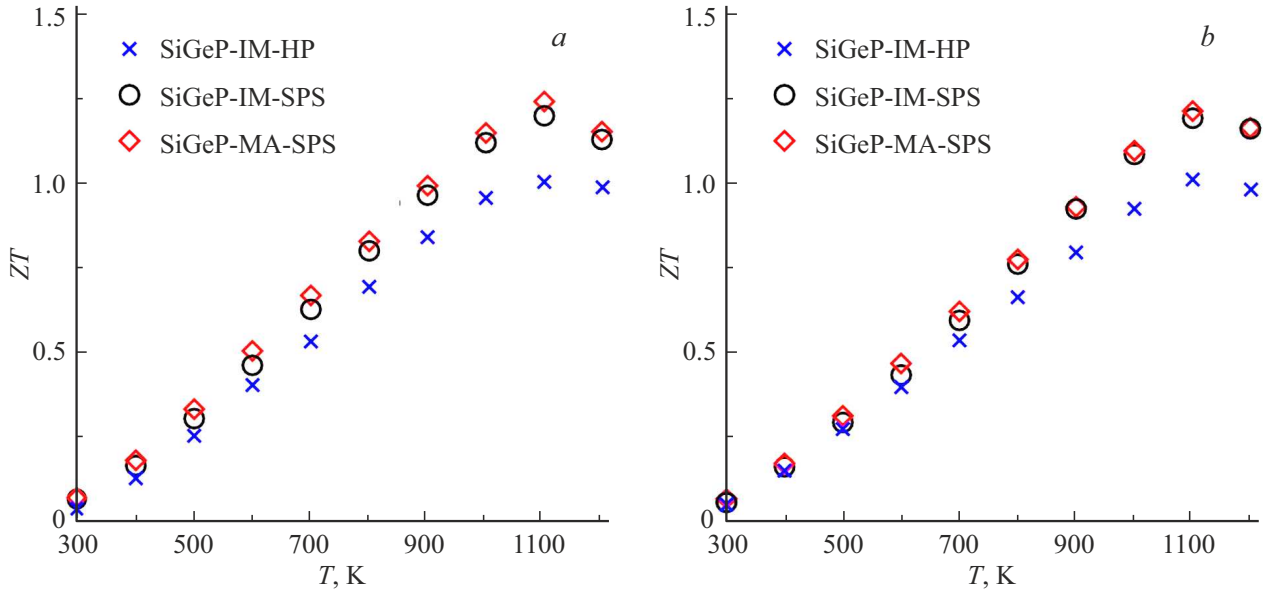

Figure 9. Temperature dependences *ZT* of materials of (*a*) *n*-type and (*b*) *p*-type.

The results of studies of temperature dependences of thermal conductivity of nanostructured and pressed thermoelectric materials are shown in Figure 7.

The nature of the temperature dependences of the thermal conductivity of the studied thermoelectric materials in the operating temperature range is similar. As the temperature increases, the thermal conductivity decreases, reaching a minimum in the temperature range where the maximum values of the thermoelectric figure of merit are observed. The experimental values of thermal conductivity for SiGe are consistent with the data from Refs. [18–20].

Changes in the thermal conductivity of SiGe-based solid solutions over the entire temperature range at which the studies were conducted do not exceed 20 %. Comparing the thermal conductivity values of classical and nanostructured thermoelectric materials, it should be noted that for nanostructured materials based on SiGe, the thermal conductivity decreases by 15–25 %. Such a decrease in thermal conductivity is determined by the scattering of phonons with an average free path on inhomogeneities with established average crystallite sizes in these materials.

The mechanism of heat transport in SiGe-based thermoelectric materials in the range of temperatures under

consideration is determined by three main components of the total thermal conductivity — lattice (κ_l), electronic (κ_{el}) and bipolar (κ_{bp}):

$$\kappa_{tot} = \kappa_l + \kappa_{el} + \kappa_{bp}. \quad (8)$$

The contribution of these components to the overall thermal conductivity was assessed using the methodology proposed in Ref. [21]. The electronic component is determined according to the Wiedemann-Franz-Lorenz law ($\kappa_{el} = L\sigma T$, where L is the Lorenz number [21,22]). The Lorentz number was calculated using the formula [23]:

$$L = 1.49 - 0.49 \cdot e^{-|s|/21} + 1.40 \cdot e^{-|s|/85}. \quad (9)$$

According to the estimate for the model with a single parabolic zone with acoustic scattering of phonons [23], the maximum error L does not exceed 0.5 % at $|s| > 10\,\mu$V/K. At low temperatures, there is no bipolar heat transport, therefore κ_l is determined by subtracting the electronic component from the total thermal conductivity: $\kappa_l = \kappa - \kappa_{el}$. Further, taking into account the temperature dependence ($\kappa_l \infty T^{-1}$), κ_l is extrapolated to the temperature range where bipolar heat transport is manifested, which is defined as follows: $\kappa_{bp} = \kappa_{tot} - \kappa_l - \kappa_{el}$.

Experimental data on thermal conductivity and the calculation results of its components for nanostructured and hot-pressed thermoelectric materials synthesized by induction melting are presented in Figure 8.

The values and temperature dependences of κ_{tot} and its components of $Si_{0.8}Ge_{0.2}$ of *n*- and *p*-types are practically the same. The value of κ_{tot}, determined mainly by the phonon component, changes insignificantly with increasing temperature, decreasing by 20 % with a minimum in the region of 1000 K. The decrease in κ_{tot} in this temperature range is due to a decrease in κ_l. The increase in thermal conductivity after this temperature is determined by the increase in the electronic component. The contribution of bipolar heat transport in the temperature range is insignificant.

As can be seen from the results obtained, the difference in the thermal conductivity values of nanostructured and hot-pressed thermoelectric materials by up to 25 % is determined by a decrease in phonon heat transport in nanostructured materials. The electronic component of nanostructured and hot-pressed materials differs slightly, which is consistent with the data on the mobility of charge carriers (Table 4).

Based on the results of measuring the thermoelectric parameters, the values of ZT for the studied materials are calculated (Figure 9).

It can be seen from the figures that the thermoelectric figure of merit of nanostructured materials is higher than that of materials obtained by classical methods by an amount correlating with a decrease in thermal conductivity in nanostructured materials. Moreover, the maximum increase in ZT is observed at temperatures above 900 K (Table 5), which correspond to the basic operating temperature range for SiGe.

Table 5. Thermoelectric figure of merit of materials

Material	$(ZT)_{max}$	T, K
SiGeP-IM-HP	1.01 ± 0.10	1117
SiGeB-IM-HP	1.02 ± 0.10	1127
SiGeP-IM-SPS	1.22 ± 0.12	1115
SiGeB-IM-SPS	1.20 ± 0.12	1135
SiGeP-MA-SPS	1.24 ± 0.13	1113
SiGeB-MA-SPS	1.22 ± 0.12	1131

The obtained values ZT for materials produced by HP are consistent with the data from Refs. [24,25]. The maximum values of ZT nanostructured thermoelectric materials correspond to the values obtained by the authors of Refs. [26–28]. The thermoelectric figure of merit of bulk nanostructured materials made from SiGe powders obtained as a result of induction melting and mechanical alloying, as well as materials of *n*-type and *p*-types of conductivity differed within measurement errors. It is important to note that ZT is higher for nanostructured materials (by 21−23 %), than for materials of the same composition obtained by hot pressing. The increase in thermoelectric figure of merit in nanostructured materials is determined by a significant decrease in phonon heat transport.

The obtained result is explained by the fact that crystallites in nanostructured thermoelectric materials significantly scatter phonons. At the same time, for charge carriers having a free path of no more than 10 nm, mobility and, accordingly, electrical conductivity decrease slightly, since they are determined by scattering on inhomogeneities of the same order, which are not dominant in the obtained nanostructured thermoelectric materials.

Conclusion

The modes were optimized and $Si_{0.8}Ge_{0.2}$ (1.8 wt.% P) of *n*-type and $Si_{0.8}Ge_{0.2}$ (0.8 wt.% B) of *p*-type were synthesized using mechanical alloying and induction melting. Volumetric samples with specified thermoelectric parameters were obtained using HP and nanostructured SPS samples. A method for obtaining fine powders with a predominance of particles less than 100 nm has been developed for SPS. Nanostructured samples were obtained from materials synthesized by induction melting and mechanical alloying. As a result of the study, it was found that the phase composition of the bulk samples obtained by HP and SPS corresponds to $Si_{0.8}Ge_{0.2}$. The average grain size is ~ 80 nm in nanostructured materials, which coincides with the average size of crystallites. It was found that the density of the nanostructured samples

is higher than that of the samples obtained by HP, and amounts to 98 % of the synthesized materials. It was found that the electrical conductivity of the nanostructured samples is 2−4 % lower than that of the HP samples at close Seebeck coefficient values. However, a significant decrease in thermal conductivity (up to 25 %) in nanostructured materials made it possible to increase their thermoelectric figure of merit in the temperature range of 1070−1170 K to 1.24−0.13 for *n*-type and up to 1.22−0.12 for *p*-type. These values of ZT are higher by 21 % compared to the materials obtained by HP. As a result of the calculation of the components of thermal conductivity, it is shown that its decrease in nanostructured materials is determined by a decrease in phonon heat transport. Thus, the efficiency of nanostructuring of the considered thermoelectric materials is shown in order to increase ZT.

Funding

This study was supported financially by the Russian Science Foundation (project 24-19-00158).

Conflict of interest

The authors declare that they have no conflict of interest.

References

[1] X.-L. Shi, J. Zou, Z.-G. Chen. Chem. Rev. **120**, *15*, 7399 (2020).
[2] M.Yu. Shtern, M.S. Rogachev, A.A. Sherchenkov, Yu.I. Shtern. Materials Today: Proceedings **20**, 295 (2020).
[3] J. He, K. Li, L. Jia, Y. Zhu, H. Zhang, J. Linghu. Applied Thermal Engineering **236**, 121813 (2024).
[4] Z. Wu, S. Zhang, Z. Liu, E. Mu, Z. Hu. Nano Energy **91**, 106692 (2022).
[5] P. Sauerschnig, P. Jood, M. Ohta. Adv Materials Technologies **8**, *5*, 2201295 (2023).
[6] Z. Dashevsky, A. Jarashneli, Y. Unigovski, B. Dzunzda, F. Gao, R. Shneck. Energies **15**, *11*, 3960 (2022).
[7] A.A. Ivanov, E.P. Kaplar, Y.P. Prilepo, V.V. Murav'ev, V.S. Ustinov. Nanobiotechnology reports **16**, *3*, 268 (2021).
[8] Y. Shtern, A. Sherchenkov, M. Shtern, M. Rogachev, D. Pepelyaev. Materials Today Communications **37**, 107083 (2023).
[9] A.P. Novitskii, V.V. Khovaylo, T. Mori. Nanobiotechnology reports. **16**, *3*, 324 (2021).
[10] D. Palaporn, S. Tanusilp, Y. Sun, S. Pinitsoontorn, K. Kurosaki. Mater. Adv. **5**, *13*, 5351 (2024).
[11] A.A. Sherchenkov, Yu.I. Shtern, M.Yu. Shtern, M.S. Rogachev. Nanotechnol Russia **11**, *7−8*, 387 (2016).
[12] Z. Dashevsky, I. Horichok, M. Maksymuk, A.R. Muchtar, B. Srinivasan, T. Mori. J. Am Ceram Soc. **105**, *6*, 4500 (2022).
[13] A.I. Gusev. Nanomaterialy, nanostruktury, nanotekhnologii. Fizmatlit, 2009, p. 416 (in Russian).
[14] M.Yu. Shtern. In 2019 IEEE Conference of Russian Young Researchers in Electrical and Electronic Engineering (EIConRus). IEEE: Saint Petersburg and Moscow, Russia. (2019).
[15] T. Hayashi, M. Sekine, J. Suzuki, Y. Horio, H. Takizawa. Mater. Trans. **48**, *10*, 2724 (2007).
[16] M.Yu. Shtern, A.A. Sherchenkov, Yu.I. Shtern, M.S. Rogachev, A.V. Babich. Nanobiotechnology reports **16**, *3*, 363 (2021).
[17] N. Tabachkova, M. Shtern, A. Sherchenkov, Y. Shtern, M. Rogachev, V. Panchenko, A. Babich, M. Voronov, M. Tapero, E. Korchagin. Solid State Sciences **154**, 107609 (2024).
[18] Y. Li, J. Han, Q. Xiang, C. Zhang, J. Li. J. Mater Sci: Mater Electron **30**, *10*, 9163 (2019).
[19] S. Wongprakarn, S. Pinitsoontorn, S. Tanusilp, K. Kurosaki. Materials Science in Semiconductor Processing **88**, 239 (2018).
[20] J. Li, J. Han, T. Jiang, L. Luo, Y. Xiang. Journal of Elec Materi **47**, *8*, 4579 (2018).
[21] M.S. Rogachev, M.Yu. Shtern, Yu.I. Shtern. Nanobiotechnology reports **16**, *3*, 308 (2021).
[22] T. Zhu, Y. Liu, C. Fu, J.P. Heremans, J.G. Snyder, X. Zhao. Advanced Materials **29**, *14*, 1605884 (2017).
[23] H.-S. Kim, Z.M. Gibbs, Y. Tang, H. Wang, G.J. Snyder. APL Materials **3**, *4*, 041506 (2015).
[24] S. Ahmad, R. Basu, P. Sarkar, A. Singh, A. Bohra, S. Bhattacharya, R. Bhatt, K.N. Meshram, S. Samanta, P. Bhatt, M. Navaneethan, Y. Hayakawa, A.K. Debnath, S.K. Gupta, D.K. Aswal, K.P. Muthe, S.C. Gadkari. Materialia **4**, 147 (2018).
[25] S. Ahmad, A. Singh. Physica B: Condensed Matter **674**, 415534 (2024).
[26] Y. Li, J. Li, J. Du, J. Han, Q. Xiang, C. Zhang. Journal of Nuclear Materials **528**, 151856 (2020).
[27] K. Meng, L.-M. Zhao, N.-Y. Zhang, Z.-F. Zhang, W.-X. Shen, Y.-W. Zhang, B. Wan, C. Fang, L.-C. Chen, Q.-Q. Wang, J.-L. He, X.-P. Jia. Rare Met. **41**, *12*, 4156 (2022).
[28] A. Nozariasbmarz, P. Roy, Z. Zamanipour, J.H. Dycus, M.J. Cabral, J.M. LeBeau, J.S. Krasinski, D. Vashaee. APL Materials **4**, *10*, 104814 (2016).

Translated by A.Akhtyamov